Advanced Robotics

ISSN: 0169-1864 (Print) 1568-5535 (Online) Journal homepage: http://www.tandfonline.com/loi/tadr20

Online Walking Pattern Generation and Its Application to a Biped Humanoid Robot — KHR-3 (HUBO)

Ill-Woo Park , Jung-Yup Kim & Jun-Ho Oh

To cite this article: Ill-Woo Park , Jung-Yup Kim & Jun-Ho Oh (2008) Online Walking Pattern Generation and Its Application to a Biped Humanoid Robot — KHR-3 (HUBO), Advanced Robotics, 22:2-3, 159-190, DOI: 10.1163/156855308X292538

To link to this article: https://doi.org/10.1163/156855308X292538

Published online: 02 Apr 2012.

VSP

Advanced Robotics 22 (2008) 159–190

ADVANCED ROBOTICS
www.brill.nl/ar

Full paper

Online Walking Pattern Generation and Its Application to a Biped Humanoid Robot — KHR-3 (HUBO)

Ill-Woo Park *, **Jung-Yup Kim and Jun-Ho Oh**

HUBO Laboratory, Humanoid Robot Research Center, Department of Mechanical Engineering, Korea Advanced Institute of Science and Technology, 373-1 Guseong-dong, Yuseong-gu, Daejeon 305-701, South Korea

Received 15 December 2006; accepted 23 April 2007

Abstract

The authors propose a simple on-line method for generating a walking pattern for the biped humanoid robot KHR-3 (HUBO). The problem of realizing a walking action in humanoid robots involves two components: generation of the basic walking pattern and the compensation required to maintain the robot's balance. Dynamic walking can be realized by incorporating the real-time stabilizing control algorithm developed for KHR-1, KHR-2 and KHR-3. The walking pattern of KHR-3 has four modes: forward/backward, left/right, curved walking and turning around. In the previous pattern generation of the KHR series, the step time and stride of the robot were fixed, and the walking modes, step time and action of stride without stopping could not be changed. Hence, the flexibility of the walking pattern of the robot needed to be upgraded. The walking pattern in this paper allows variation in the walking mode, step time and stride for each step. The pattern uses a simple mathematical form of trajectory curves, specifically the sine, cosine, linear and third-order polynomial curves, and the superposition of these curves is used to minimize the complexity and burden of the computation. The authors used a third-order polynomial to generate the trajectory of the robot's pelvis. With the aid of a simplified zero-moment point (ZMP) equation, the pelvis trajectories have a direct relationship with the ZMP trajectories. An effective means of generating the trajectories is introduced, and the scheme is verified experimentally under various walking conditions that take into account the step time and stride. The experimental platform, which has human-like features and movement, is briefly introduced here. With a simple kinematical structure and distributed control hardware architecture, the platform was designed to consume relatively low levels of energy. Moreover, the scheme for generating the trajectory is realized for variations to flexible walking.

Keywords

Biped walking, walking pattern generation, humanoid, dynamic walking, HUBO

* To whom correspondence should be addressed. E-mail: mrquick@mclab3.kaist.ac.kr

 DOI:10.1163/156855308X292538

1. Introduction

Many researchers have reported impressive results in the humanoid robotics field. Some robots walk and move nearly as well as humans, and are more human-friendly than other types of robots. Many humanoid robots have recently been developed [1–8]. The Japanese robots P2, P3 and ASIMO of Honda, the WABIAN series of Waseda University, H6 and H7 of Tokyo University, and the HRP series of AIST are good examples of human-sized biped humanoid robots. Studies regarding biped walking tend to focus on mobility and human interaction. Much progress has been reported in the development of fast and free walking or running robots, as well as in mobility and the implementation of artificial intelligence for functions such as visual recognition, voice recognition and navigation.

Biped walking involves the two processes shown in Fig. 1: walking pattern generation [9–16] and real-time control [17–21]. Walking patterns based on the zero-moment point (ZMP) are usually generated by off-line simulations with accurate information of the robot system such as the masses and moments of inertia of the robot [9, 12, 13]. This approach can generate a stable walking pattern as it is based on precise information about the system [11–13, 15]. The pattern itself is theoretically stable, but practically weak in terms of handling disturbances of the system due to unmodeled environmental conditions or the inaccuracy of the model. For this reason, implementation of a real-time feedback controller is necessary [17–21]. Although the importance of feedback controllers is generally accepted nowadays, the major contribution of walking is to generate a suitable walking pattern (or a desired ZMP trajectory generation). A scheme that generates a flexible walking pattern as well as an effective method of the ZMP trajectory generation is proposed for this.

There are two approaches to the generation of biped walking patterns. The first approach is a forward approach. After the motion pattern has been planned, a checking process should determine whether or not the calculated ZMP is in the supporting polygon [9, 11, 15]. This approach to the generation of walking patterns has flexibility and can be applied to various walking situations, such as avoiding obstacles or following an object, as the pattern is designed to be more suitable for walking

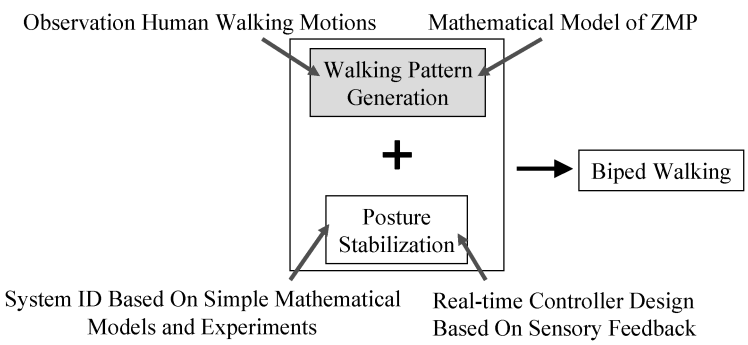

Figure 1. Realization of biped walking.

tasks such as forward walking, side walking, and turning with a given step time, stride and mode. However, there is less confidence in the physical stability in the absence of a calculation of the ZMP equation or an experiment. Hence, a simple and effective solution to this problem is needed.

The second approach to the generation of biped walking patterns is an inverse approach, which uses various methods to determine an acceptable pattern after the desired ZMP has been designed [12, 15]. This approach can generate a stable walking pattern, but the complexity of the pattern generation process increases. As a result, the adaptability of the walking action decreases in various situations such as avoiding obstacles or following an object due to the time-consuming and burdensome nature of the ZMP calculation.

The complexity of designing a walking pattern is due to the complexity of ZMP equations, which require information regarding the multi-mass/moment of inertia and the position/angular acceleration. The first approach for the flexibility of a walking task is utilized. To have the effectiveness of a stability check scheme, the biped robot used in this study was modeled on the simple inverted pendulum presented in Refs [14, 15]. With this model, the ZMP equation is simple. The walking pattern was designed with a simplified ZMP equation and a third-order polynomial method was used for the pelvis trajectory. Although other researchers commonly use a third-order polynomial method for the pelvis curve, the desired ZMP trajectory was generated by updating the boundary condition (start and end conditions in each step). Furthermore, a direct one-to-one relationship with the pelvis trajectory is proposed for effectiveness of the gait design. The results verify that the desired ZMP trajectory conforms with the pelvis center trajectory in terms of a direct and simple mathematical relationship. The forward approach to generating a walking pattern is equivalent to the inverse approach. Once the desired ZMP is designed, the pelvis trajectory can be obtained automatically and *vice versa*. This is explained in Section 2.

In Section 3, the methodology of planning the trajectory for the center of the pelvis and the position of the ankle is described. The first requirement was to develop a method that could generate flexible walking patterns in real-time and that could be updated with every step. This scheme supports more general walking situations. The parameters and conditions, such as the sway, stride, step time, direction and walking mode, must be defined and updated before the next step starts to realize the variable walking patterns. The trajectory is defined by the boundary conditions (position and velocity) at the beginning and end of the step. The shape of the third-order polynomial curve, which can be updated easily under changeable step conditions by modifying the boundary conditions, remains smooth. To enhance the walking performance, the shape factors of the trajectory were also used. These can easily be modified.

In the remainder of this paper, the verification of the proposed scheme for generating walking patterns is discussed. Experimental results are presented for forward

and side walking with a variable step time (0.7, 0.8 and 0.95 s) and step length (forward: 10, 20, 25 (0.7 and 0.8 s) and 30 cm (0.95 s); side: 5 and 7 cm). The parameters and shape factors for walking were found by means of a simplified ZMP trajectory and experiment. With this scheme, it is possible to change the walking frequency and step length arbitrarily within the above conditions.

2. ZMP and Pelvis Center Trajectory

A dynamic ZMP equation can be simplified and divided into two parts, (1) and (2), using the single inverted pendulum model (Figs 2–5). When it is assumed that the

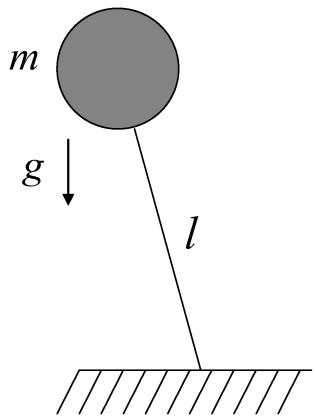

Figure 2. Inverted pendulum model.

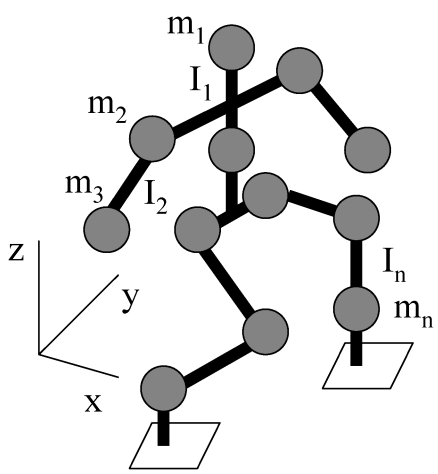

Figure 3. General model of a biped.

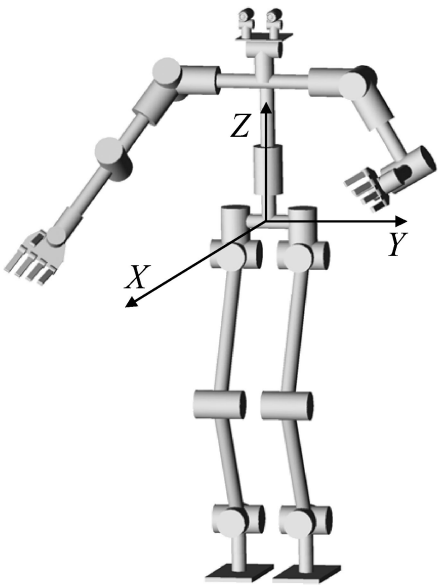

Figure 4. Schematic of the robot (X, Y and Z represent the inertial reference frame that initially originated at the pelvis center).

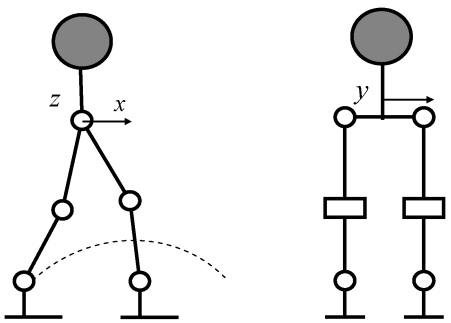

Figure 5. Coordinate description (x, y and z represent the fixed coordinate frame for the center of the pelvis). (a) Sagittal view. (b) Coronal view.

Z-motion of the pelvis or center of gravity does not occur, the ZMP equation can be simplified as (1) and (2):

$$x_{\text{zmp}} = \frac{\sum_{i=1}^{n} m_i(\ddot{z}_i + g)x_i - \sum_{i=1}^{n} m_i \ddot{x}_i z_i - \sum_{i=1}^{n} I_{iy}\ddot{\Omega}_{iy}}{\sum_{i=1}^{n} m_i(\ddot{z}_i + g)}$$
$$\approx x_{\text{CG}} - \ddot{x}_{\text{CG}}\frac{l}{g} \tag{1}$$

$$y_{\mathrm{zmp}} = \frac{\sum_{i=1}^{n} m_i(\ddot{z}_i + g)y_i - \sum_{i=1}^{n} m_i \ddot{y}_i z_i - \sum_{i=1}^{n} I_{ix}\ddot{\Omega}_{ix}}{\sum_{i=1}^{n} m_i(\ddot{z}_i + g)}$$
$$\approx y_{\mathrm{CG}} - \ddot{y}_{\mathrm{CG}}\frac{l}{g}, \tag{2}$$

where m_i is the mass, x_i, y_i, z_i is the position, I_i is the moment of inertia and Ω_i is the angular velocity. In (1) and (2), the first terms (x_{CG} and y_{CG}) denote the static components and the second terms ($\ddot{x}_{\mathrm{CG}}$ and $\ddot{y}_{\mathrm{CG}}$) represent the dynamic components of the ZMP. A third-order polynomial interpolation is proposed for the design of the ZMP trajectories. A polynomial can be easily used to generate a walking pattern for various walking conditions, and the walking pattern and ZMP trajectory have a simple and direct relationship. For this reason, the desired ZMP trajectory was designed to determine the trajectory of the center of the pelvis.

2.1. Sagittal View

For the design stage of the ZMP trajectory, a basic ZMP trajectory with the form of (3) during a step is proposed. Equation (3) is a third-order polynomial position and its time-derivative (velocity) trajectory. The time scale can be normalized so that a step starts at $t_{\mathrm{N}} = 0$ and ends at $t_{\mathrm{N}} = 1$ without loss of generality:

$$x_{\mathrm{zmp}} = \sum_{i=0}^{3} b_i t_{\mathrm{N}}^i, \quad \dot{x}_{\mathrm{zmp}} = \sum_{i=1}^{3} i \cdot b_i t_{\mathrm{N}}^{i-1},$$
$$\text{where } 0 \leqslant t_{\mathrm{N}} \leqslant 1 \tag{3}$$

$$\begin{bmatrix} b_3 \\ b_2 \\ b_1 \\ b_0 \end{bmatrix} = \begin{bmatrix} 0 & 0 & 0 & 1 \\ 0 & 0 & 1 & 0 \\ 1 & 1 & 1 & 1 \\ 3 & 2 & 1 & 0 \end{bmatrix}^{-1} \begin{bmatrix} x_{\mathrm{zmp},0} \\ \dot{x}_{\mathrm{zmp},0} \\ x_{\mathrm{zmp},1} \\ \dot{x}_{\mathrm{zmp},1} \end{bmatrix}$$
$$= \begin{bmatrix} 2 & 1 & -2 & 1 \\ -3 & -2 & 3 & -1 \\ 0 & 1 & 0 & 0 \\ 1 & 0 & 0 & 0 \end{bmatrix} \begin{bmatrix} x_{\mathrm{zmp},0} \\ \dot{x}_{\mathrm{zmp},0} \\ x_{\mathrm{zmp},1} \\ \dot{x}_{\mathrm{zmp},1} \end{bmatrix}. \tag{4}$$

The boundary conditions of the ZMP at the lifting and landing of the step are $x_{\mathrm{zmp},0}$, $\dot{x}_{\mathrm{zmp},0}$, $x_{\mathrm{zmp},1}$ and $\dot{x}_{\mathrm{zmp},1}$. With this form of this equation and these boundary conditions, it is possible to design a smooth ZMP trajectory curve by assigning the proper values to $x_{\mathrm{zmp},0}$, $\dot{x}_{\mathrm{zmp},0}$, $x_{\mathrm{zmp},1}$ and $\dot{x}_{\mathrm{zmp},1}$ in (4). The coefficients can then be derived from the given boundary conditions.

By assuming that the x-coordinate of the center of gravity (x_{CG}) is identical to the center of the pelvis ($\tilde{x}_{\mathrm{P}}$), it can be assumed from (1) and (3) that the pelvis trajectory, $\tilde{x}_{\mathrm{P}}$, has the same form as (3) but with different coefficients:

$$x_{\mathrm{CG}} = \tilde{x}_{\mathrm{P}}(t) = \sum_{i=0}^{3} a_i t_{\mathrm{N}}^i, \quad \text{where } 0 \leqslant t_{\mathrm{N}} \leqslant 1. \tag{5}$$

By inserting (3) and (5) into (1), the following expression is obtained:

$$\begin{aligned} x_{\mathrm{zmp}} &= \sum_{i=0}^{3} b_i t_{\mathrm{N}}^i \\ &= \left(a_0 - 2a_2\frac{l}{g}\right) + \left(a_1 - 6a_3\frac{l}{g}\right)t_{\mathrm{N}} + a_2 t_{\mathrm{N}}^2 + a_3 t_{\mathrm{N}}^3. \end{aligned} \tag{6}$$

As shown in (6), there is an explicit match between the coefficients of the ZMP and the trajectory of the center of the pelvis. Moreover, the relationship between the boundary conditions of the ZMP and those of the trajectory of the center of the pelvis, which is shown in (7), can easily be calculated by equating the coefficients of (6) with each other.

$$\begin{bmatrix} x_{\mathrm{zmp},0} \\ \dot{x}_{\mathrm{zmp},0} \\ x_{\mathrm{zmp},1} \\ \dot{x}_{\mathrm{zmp},1} \end{bmatrix} = \begin{bmatrix} 1+\frac{6l}{g} & \frac{4l}{g} & -\frac{6l}{g} & \frac{2l}{g} \\ -\frac{12l}{g} & 1-\frac{6l}{g} & \frac{12l}{g} & -\frac{6l}{g} \\ -\frac{6l}{g} & -\frac{2l}{g} & 1+\frac{6l}{g} & -\frac{4l}{g} \\ -\frac{12l}{g} & -\frac{6l}{g} & \frac{12l}{g} & 1-\frac{6l}{g} \end{bmatrix} \begin{bmatrix} \tilde{x}_{\mathrm{P}}(0) \\ \dot{\tilde{x}}_{\mathrm{P}}(0) \\ \tilde{x}_{\mathrm{P}}(1) \\ \dot{\tilde{x}}_{\mathrm{P}}(1) \end{bmatrix}. \tag{7}$$

2.2. Coronal View

With a similar process in the previous sagittal view case (x_{zmp} derivation case), the relation between y_{zmp} and $\tilde{y}_{\mathrm{P}}$ is simply derived. As shown in Fig. 6, the coronal view differs from the sagittal view in terms of the time division for the trajectory generation and d_1. The time division is needed to determine the velocity and the maximum amplitude of the ZMP (or the center of the pelvis) at $t_{\mathrm{N}} = 1/2$ (where the lifting foot has its maximum height). The d_1 factor represents the staying ratio

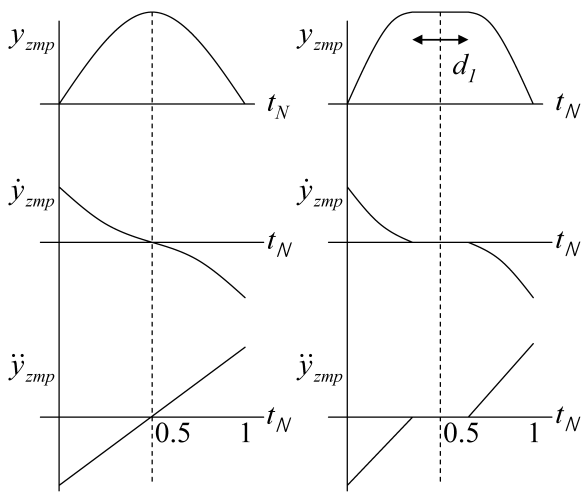

Figure 6. Position, velocity and acceleration curve of the ZMP (the ZMP trajectory is designed with a third-order polynomial).

of the ZMP. Using d_1, a sudden sign change of acceleration during the interval was avoided to increase the stability of the robot.

The relationships between y_{zmp} and $\tilde{y}_{\mathrm{P}}$ can be derived by redefining the time scale. In Section 3.2, the time scale, $\bar{t}$, in (18) was utilized to consider d_1 and the one step interval was divided into two. The expression $0 \leqslant t_{\mathrm{N}} < 1/2$ is the first interval of (8) and $1/2 \leqslant t_{\mathrm{N}} \leqslant 1$ is the second interval of (8). The relationship between the boundary conditions of the ZMP trajectory and the trajectory of the center of the pelvis is presented in (9) and (10), respectively:

$$y_{\mathrm{zmp}} = \sum_{i=0}^{3} \tilde{b}_i \bar{t}^i \tag{8}$$

$$\begin{aligned}\begin{bmatrix} \tilde{b}_3 \\ \tilde{b}_2 \\ \tilde{b}_1 \\ \tilde{b}_0 \end{bmatrix} &= \begin{bmatrix} 0 & 0 & 0 & 1 \\ 0 & 0 & 1 & 0 \\ 1/8 & 1/4 & 1/2 & 1 \\ 3/4 & 1 & 1 & 0 \end{bmatrix}^{-1} \begin{bmatrix} y_{\mathrm{zmp},0} \\ \dot{y}_{\mathrm{zmp},0} \\ y_{\mathrm{zmp},1/2} \\ \dot{y}_{\mathrm{zmp},1/2} \end{bmatrix} \\ &= \begin{bmatrix} 16 & 4 & -16 & 4 \\ -12 & -4 & 12 & -2 \\ 0 & 1 & 0 & 0 \\ 1 & 0 & 0 & 0 \end{bmatrix} \begin{bmatrix} y_{\mathrm{zmp},0} \\ \dot{y}_{\mathrm{zmp},0} \\ y_{\mathrm{zmp},1/2} \\ \dot{y}_{\mathrm{zmp},1/2} \end{bmatrix},\end{aligned}$$

where $0 \leqslant t_{\mathrm{N}} < 1/2$

$$\begin{aligned}\begin{bmatrix} \tilde{b}_3 \\ \tilde{b}_2 \\ \tilde{b}_1 \\ \tilde{b}_0 \end{bmatrix} &= \begin{bmatrix} 1/8 & 1/4 & 1/2 & 1 \\ 3/4 & 1 & 1 & 0 \\ 1 & 1 & 1 & 1 \\ 3 & 2 & 1 & 0 \end{bmatrix}^{-1} \begin{bmatrix} y_{\mathrm{zmp},1/2} \\ \dot{y}_{\mathrm{zmp},1/2} \\ y_{\mathrm{zmp},1} \\ \dot{y}_{\mathrm{zmp},1} \end{bmatrix} \\ &= \begin{bmatrix} 16 & 4 & -16 & 4 \\ -36 & -10 & 36 & -8 \\ 24 & 8 & -24 & 5 \\ -4 & -2 & 5 & -1 \end{bmatrix} \begin{bmatrix} y_{\mathrm{zmp},1/2} \\ \dot{y}_{\mathrm{zmp},1/2} \\ y_{\mathrm{zmp},1} \\ \dot{y}_{\mathrm{zmp},1} \end{bmatrix},\end{aligned}$$

where $1/2 \leqslant t_{\mathrm{N}} \leqslant 1$

$$M = \begin{bmatrix} 1 + \frac{24l}{g} & \frac{8l}{g} & -\frac{24l}{g} & \frac{4l}{g} \\ -\frac{96l}{g} & 1 - \frac{24l}{g} & \frac{96l}{g} & -\frac{24l}{g} \\ -\frac{24l}{g} & -\frac{4l}{g} & 1 + \frac{24l}{g} & -\frac{8l}{g} \\ -\frac{96l}{g} & -\frac{24l}{g} & \frac{96l}{g} & 1 - \frac{24l}{g} \end{bmatrix} \tag{9}$$

$$\begin{bmatrix} y_{\mathrm{zmp},0} \\ \dot{y}_{\mathrm{zmp},0} \\ y_{\mathrm{zmp},1/2} \\ \dot{y}_{\mathrm{zmp},1/2} \end{bmatrix} = M \begin{bmatrix} \tilde{y}_{\mathrm{P}}(0) \\ \dot{\tilde{y}}_{\mathrm{P}}(0) \\ \tilde{y}_{\mathrm{P}}(1/2) \\ \dot{\tilde{y}}_{\mathrm{P}}(1/2) \end{bmatrix}, \quad \text{where } 0 \leqslant t_{\mathrm{N}} < 1/2;$$

$$\begin{bmatrix} y_{\mathrm{zmp},1/2} \\ \dot{y}_{\mathrm{zmp},1/2} \\ y_{\mathrm{zmp},1} \\ \dot{y}_{\mathrm{zmp},1} \end{bmatrix} = M \begin{bmatrix} \tilde{y}_{\mathrm{P}}(1/2) \\ \dot{\tilde{y}}_{\mathrm{P}}(1/2) \\ \tilde{y}_{\mathrm{P}}(1) \\ \dot{\tilde{y}}_{\mathrm{P}}(1) \end{bmatrix}, \quad \text{where } 1/2 \leqslant t_{\mathrm{N}} \leqslant 1. \tag{10}$$

In this section, the design of the trajectory for the center of the pelvis was confirmed to be equivalent to the design of the ZMP trajectory when the inverted pendulum model is used while assuming a flat ground condition and a third-order polynomial interpolation. The interpolation method is useful for generating the desired ZMP under various conditions, as a smooth trajectory is made by updating the boundary conditions for each step. With the interpolation method, it is not necessary to analyze the full ZMP equation when designing the walking pattern. Rather, simplified equations are used for an effective design of the center of the pelvis and the ZMP trajectory. To calculate the boundary conditions of the ZMP trajectory, it is necessary to determine the ZMP trajectory curve with respect to the boundary conditions of the trajectory of the center of the pelvis, and *vice versa*, as the coefficients of the polynomials are automatically matched. In the next section, some parameters and factors that can be tuned for various walking conditions (such as the step time, stride and mode) are proposed.

3. Generation of the Walking Pattern

For convenience, the position of the center of the pelvis and the ankle in terms of the sagittal, coronal, and top planes is described here. Figure 7 shows the sagittal and coronal view as well as the fixed coordinate frame of the center of the pelvis.

The scheme for the on-line generation of the walking pattern generates the trajectories for the input parameters, which are the sway amplitude, step time, stride, mode and direction in real-time. The input parameters are prepared before the step started and are updated at the start of each step. Biped walking has two basic prob-

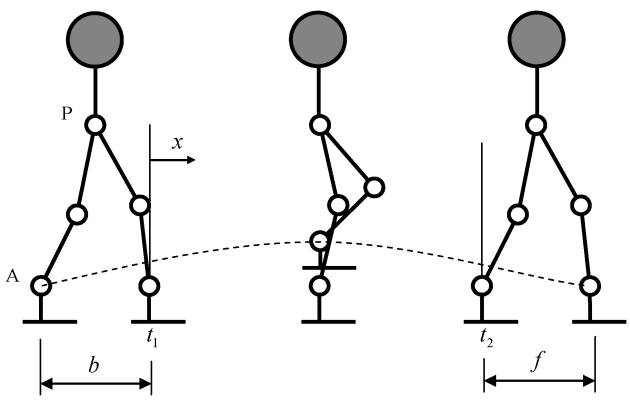

Figure 7. Coordinate description in the X-direction.

lems: generation of the kinematical position path, and the problem of designing a dynamic controller that can yield a clear, practical and simple solution.

To solve the problem of generating the kinematical position path, it is necessary to meet the following requirements:

(i) The robot must be easy to operate. There should be minimal input from the operator with respect to the step time, stride and mode (forward/backward, left/right, among others) as well as commands such as start and stop.

(ii) The curves must have a simple form and smooth property. The curves should be clear and simple. The trajectory of the pattern should have a simple analytic form and be differentiable due to the continuity of the velocity. After the curves of the walking pattern have been formulated, the parameters for every step are updated.

(iii) The calculation must be easy to implement in an actual system.The calculation burden and memory use should be small, and the pattern modification should be flexible.

(iv) The number of factors and parameters *that need to be tuned must be small.* The walking pattern must be tuned to increase the walking performance. The acceptability of the pattern can be validated by experiments that need time and labor. The experiments can be effective if the number of factors and parameters is small.

The position of each motor is controlled by feedback from a servo motor encoder. To control all the motors, the main computer must send joint position control commands in hard real time. In KHR-3, the main computer simultaneously sends the reference position data to all of the motor controllers every 10 ms (100 Hz). Each servo motor controller then generates a fine position command every millisecond by linear interpolation with the reference position data from the main controller. In the opposite direction, the sensory devices send sensory information back to the main controller at a frequency of 100 Hz. Figure 8 shows an outline of the motion generation and control process.

3.1. Sagittal View

$$\tilde{x}_{\mathrm{A}}(t) = (b+f)\left(\frac{t-(t_1+d/2)}{(t_2-d/2)-(t_1+d/2)} - \frac{1}{2\pi}\sin\left(2\pi\frac{t-(t_1+d/2)}{(t_2-d/2)-(t_1+d/2)}\right)\right) - b \tag{11}$$

$$\tilde{x}_{\mathrm{P}}(t) = \sum_{i=0}^{3} a_i \left(\frac{t-t_1}{t_2-t_1}\right)^i. \tag{12}$$

The symbol $\tilde{x}$ in Fig. 7 is located on the front supporting foot while the other leg swings in the X-direction. The parameter t_1 is the start time of a swing from the double-support phase (DSP) and t_2 is the end time of a swing to the other DSP. The stride inputs b and f are the positions of the swinging leg at t_1 and t_2, and d is the

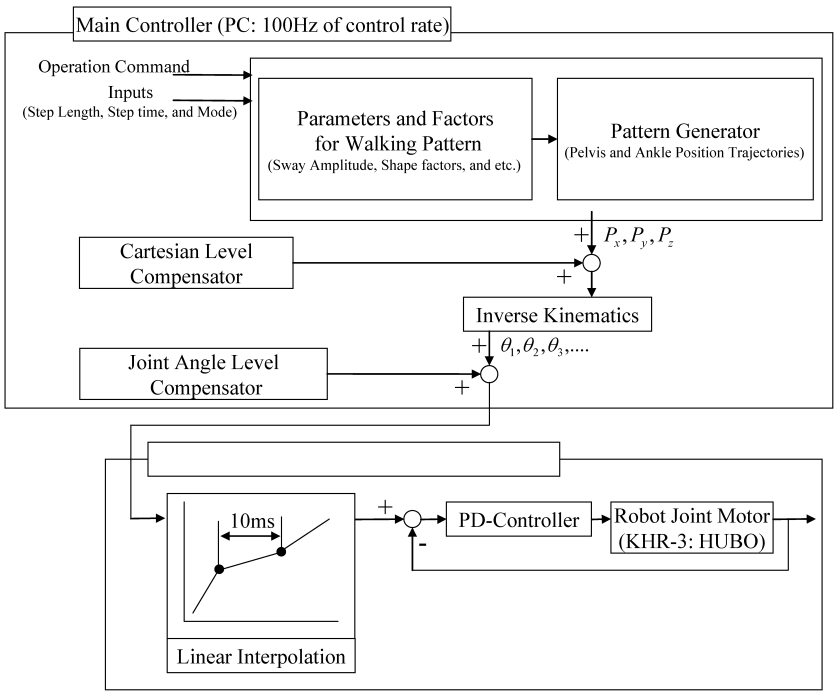

Figure 8. Motion generation and control process of KHR-3.

DSP time. It is assumed that the center position of the pelvis is at the center of the two ankles at t_1 and t_2. First, the trajectories of the pelvis and the swinging leg were generated in this local coordinate frame, $\tilde{x}$, and the trajectories were implemented in the robot on the basis of the x frame by translating the coordinate frame (see Figs 4 and 5). Equation (11) shows the ankle position and (12) shows the center position of the pelvis in the local coordinate frame.

Equation (11) is a cycloid curve, which is the superposition of a linear curve and a sine curve. This function has zero velocity at the start and the end, and it has its maximum velocity in the swinging phase. Equation (12) is a third-order polynomial curve. The coefficient of this curve, a_i, is calculated by the boundary conditions at the start and the end of each step. When the time-scale is normalized to $t_1 = 0$ and $t_2 = 1$, a_i could be determined. In (13), it was assumed that the position of the pelvis at t_1 and t_2 was at the center of the two ankles. The boundary conditions are the position and the velocity of the pelvis. As shown in (13), they are related to the stride inputs of b and f as well as to the shape factor, α. The velocity of the pelvis is proportional to the stride inputs and α establishes this relationship. As shown in Fig. 9, the curve shape of the pelvis position can be tuned by finding the proper α, which explains why α is referred to as a shape factor. However, the α value is limited until an unexpected reverse action takes place. The value of α affects the

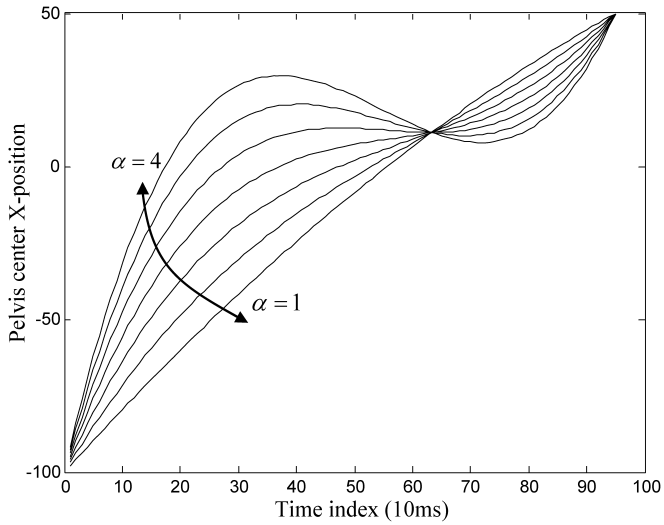

Figure 9. Example trajectory of the changing shape of the center of the pelvis with respect to the α factor.

dynamic property of forward walking; when the value is large, the pelvis moves rapidly at the start and at the end of the step, and slows when the leg swings.

$$\begin{bmatrix} \tilde{x}_{\mathrm{P}}(0) \\ \dot{\tilde{x}}_{\mathrm{P}}(0) \\ \tilde{x}_{\mathrm{P}}(1) \\ \dot{\tilde{x}}_{\mathrm{P}}(1) \end{bmatrix} = \begin{bmatrix} -b/2 \\ \alpha b \\ f/2 \\ \alpha f \end{bmatrix}. \tag{13}$$

The shape factor (α) and the inputs (b and f) were presented for continuous forward walking under the boundary condition. Hence, the design of the ZMP trajectory sought to determine the proper shape factor for various walking conditions because, as shown in Section 2, the design factors have a one-to-one relationship with the ZMP trajectory.

Figures 10 and 11 show examples of the swinging ankle and the center position of the pelvis during a single step. In Figs 10 and 11, it is assumed that the right ankle is the supporting ankle and the left ankle is the swinging ankle. When the X-direction trajectory is applied to the robot, as shown in Fig. 11, the relative left and right ankle positions are used with the pelvis center origin. These two parameters are expressed as $\hat{x}_{\mathrm{A,Support}}(t) = -\tilde{x}_{\mathrm{P}}(t)$ and $\hat{x}_{\mathrm{A,Swing}}(t) = \tilde{x}_{\mathrm{A}}(t) - \tilde{x}_{\mathrm{P}}(t)$, respectively.

The trajectory of the foot height is shown in Fig. 12. By adjusting the ratio between the lifting and landing timing, it is possible to control the speeds of the up and down motions. Fast lifting and slow landing may reduce the landing impact, but may also increase the structural vibration during the lifting motion, and *vice versa*. To reduce the landing shock, it was ensured that the value of u is not larger than 0.5.

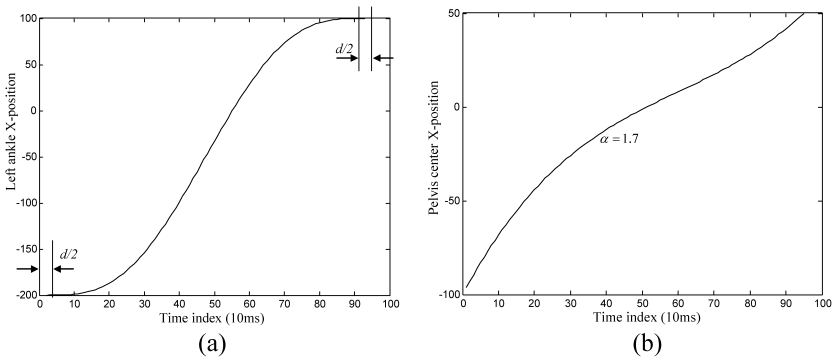

Figure 10. Example trajectories of the swinging ankle and the center of the pelvis (X-direction: $t_1 = 0$, $t_2 = 0.95$ s, $b = 200$ mm, $f = 100$ mm). (a) Position of the swinging ankle ($\tilde{x}_{\mathrm{A}}(t)$). (b) Position of the center of the pelvis ($\tilde{x}_{\mathrm{P}}(t)$).

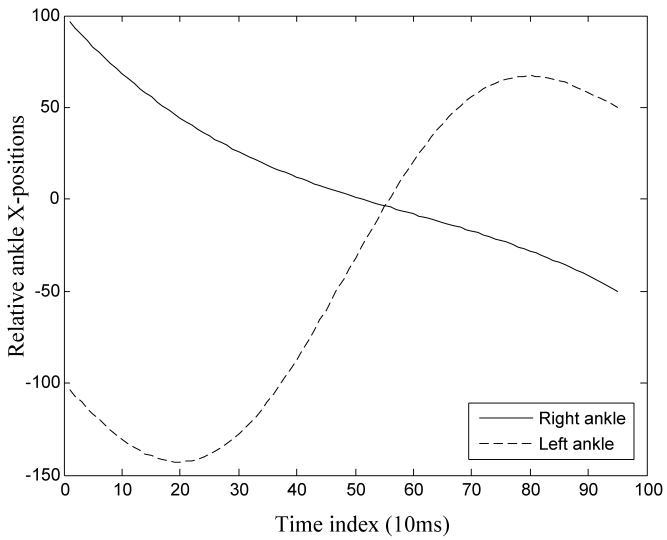

Figure 11. Example trajectory of the relative ankle positions.

3.2. Coronal View (Y-direction)

In this subsection, the coronal view of the walking trajectory is described. The descriptions of the Y-direction movement are for side walking, turning and the sway movement of the center of the pelvis.

The additive ankle position in the side walking mode is generated in two stages. The first stage involves an open stance posture, in which the ankles proceed from a ready position to an open stance position. The second stage involves recovery from an open stance to a ready position. In the ready position, which is the default posture of the robot before the start of the walking motion and after the end of the walking motion, the robot's legs are slightly bent. For convenience, the stage numbers are

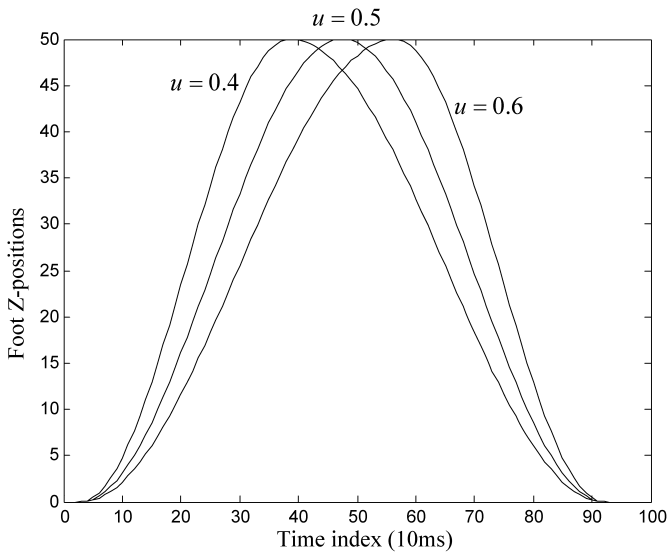

Figure 12. Profile of the changing shape of the center of the pelvis with respect to the u factor (u: up/down time ratio of the foot).

written in superscript at t and the coefficient A is positive when the robot walks to the left side. The additive ankle positions are written in (14)–(17). The coefficient A is the step length of the side walk and the middle of the step time, t_0, is $(t_1 + t_2)/2$. When these positions are implemented, the pelvis Y-position is simply added for side walking:

$$\hat{y}_{\mathrm{A_L}} = \frac{A}{4}\left(1 - \cos\left(\pi \frac{t - t_1^1}{t_2^1 - t_1^1}\right)\right) \tag{14}$$

$$\hat{y}_{\mathrm{A_R}} = \frac{-A}{4}\left(1 - \cos\left(\pi \frac{t - t_0^1}{t_2^1 - t_0^1}\right)\right) \tag{15}$$

$$\hat{y}_{\mathrm{A_L}} = \frac{A}{4}\left(1 + \cos\left(\pi \frac{t - t_1^2}{t_0^2 - t_1^2}\right)\right) \tag{16}$$

$$\hat{y}_{\mathrm{A_R}} = \frac{-A}{4}\left(1 + \cos\left(\pi \frac{t - t_1^2}{t_2^2 - t_1^2}\right)\right) \tag{17}$$

$$\bar{t} = \begin{cases} \dfrac{t_{\mathrm{N}}}{1 - d_1} & \left(0 \leqslant t_{\mathrm{N}} < \dfrac{1 - d_1}{2}\right) \\ 0.5 & \left(\dfrac{1 - d_1}{2} \leqslant t_{\mathrm{N}} < \dfrac{1 + d_1}{2}\right) \\ \dfrac{t_{\mathrm{N}} - d_1}{1 - d_1} & \left(\dfrac{1 + d_1}{2} \leqslant t_{\mathrm{N}} \leqslant 1\right) \end{cases} \tag{18}$$

$$\tilde{y}_{\mathrm{P}}(t_{\mathrm{N}}) = \sum_{i=0}^{3} \tilde{a}_i (2\bar{t})^i, \tag{19}$$

where:

$$\begin{gathered} \tilde{y}_{\mathrm{P}}(0) = 0, \quad \dot{\tilde{y}}_{\mathrm{P}}(0) = -\alpha_1 V_y \\ \tilde{y}_{\mathrm{P}}\left(\frac{1}{2}\right) = -\beta_1 S_y, \quad \dot{\tilde{y}}_{\mathrm{P}}\left(\frac{1}{2}\right) = 0 \\ \tilde{y}_{\mathrm{P}}(t_{\mathrm{N}}) = \sum_{i=0}^{3} \tilde{a}_i (2\bar{t} - 1)^i, \end{gathered} \tag{20}$$

where:

$$\tilde{y}_{\mathrm{P}}\left(\frac{1}{2}\right) = -\beta_1 S_y, \quad \dot{\tilde{y}}_{\mathrm{P}}\left(\frac{1}{2}\right) = 0, \quad \tilde{y}_{\mathrm{P}}(1) = 0, \quad \dot{\tilde{y}}_{\mathrm{P}}(1) = \alpha_1 V_y.$$

For the left and right movements of the center position of the pelvis, third-order polynomial interpolation is used, as in the case of the X-direction trajectory for the center position of the pelvis. The Y-direction trajectory of the pelvis requires more flexibility because the left and right weight shifting is related to every walking mode: forward/backward walking, side walking and turning around (Fig. 13). As described in Section 3.1, the time-scale for the pelvis trajectory was normalized as $t_1 = 0$, $t_2 = 1$ and $t_0 = 0.5$, and the normalized time, t_{N}, increased from 0 to 1. t_{N} was modified to $\bar{t}$, as shown in Fig. 14 and in (18). The trajectory, which is divided into two intervals per step, is generated with the boundary conditions given in (19) and (20). Dividing the time interval can reveal the amplitude and the velocity of the trajectory for the pelvis sway, and the division can directly affect the Y-direction ZMP, which can be defined at $t_1 = 0$, $t_2 = 1$ and $t_0 = 0.5$. If the time is not divided, the sway amplitude using the interpolation method cannot be guaranteed;

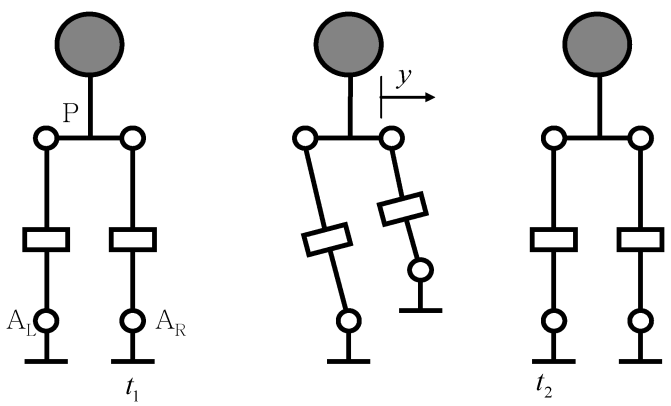

Figure 13. Coordinate description in the Y-direction ($\tilde{y}$ is the ground fixed coordinate that initially originates at the center of the pelvis).

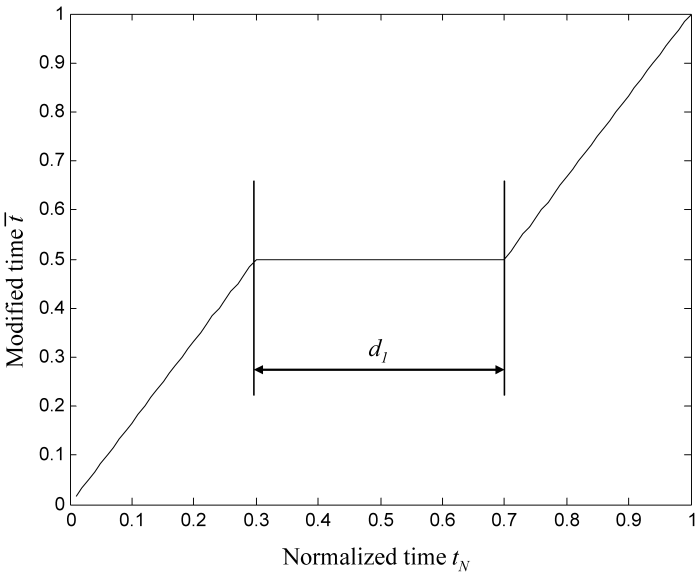

Figure 14. Time modification for the pelvis Y-direction trajectory.

furthermore, d_1 helps the ZMP to stay in the supporting foot during the single-support phase (SSP).

There are three shape factors in the curve shown in Fig. 15 (α_1, β_1 and d_1). The α_1 factor is the velocity multiplier for the start and end of each step, and the β_1 factor is an amplitude multiplier at $t_{\mathrm{N}} = 1/2$. These two factors are for the standard value modification of V_y and S_y in different walking modes or speeds, although the default value is 1 for forward walking. The d_1 factor makes it possible to extend the ZMP staying time in the SSP without changing the entire pattern. Suitable values of S_y, V_y, α_1, β_1 and d_1 were determined for the forward and side walking modes. The ankle positions relative to the center of the pelvis can be translated and applied using $\hat{y}_{\mathrm{A_L}} = \tilde{y}_{\mathrm{A_L}} + \tilde{y}_{\mathrm{P}}$ and $\hat{y}_{\mathrm{A_R}} = \tilde{y}_{\mathrm{A_R}} + \tilde{y}_{\mathrm{P}}$. Figure 16 shows an example of the trajectory of the center of the pelvis in a single forward step. Figure 17 shows an example of the ankle positions and the center position of the pelvis in the side walking mode. This approach has a simple and organized type of trajectory function, and offers flexibility through the use of the parameters and factors. The parameters and factors for each walking condition are updated before the step starts.

3.3. Top View (Z-direction)

The turning gait is realized by imposing the hip-yaw angle shown in Fig. 18 for small strides to the side, as was done in the previous KHR series [17–21]. By turning at an angle of θ, as shown in Fig. 19, the robot can walk sideways with a side stride of 'L' to prevent interference between the feet. In addition, with values of $\theta/2$ at the left yaw and $-\theta/2$ at the right yaw, the joints of the robot turn in an open stance stage and recover to zero in the recovering stage. For the joint path, the cosine

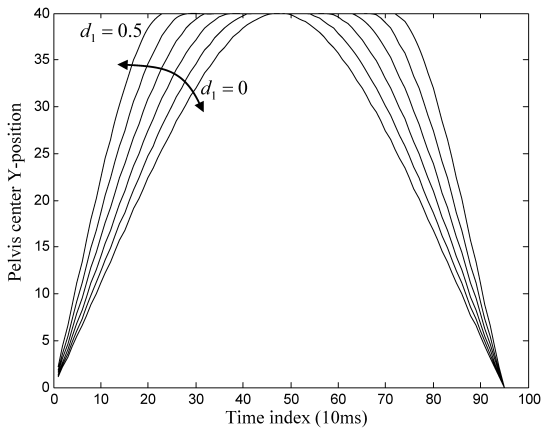

(a)

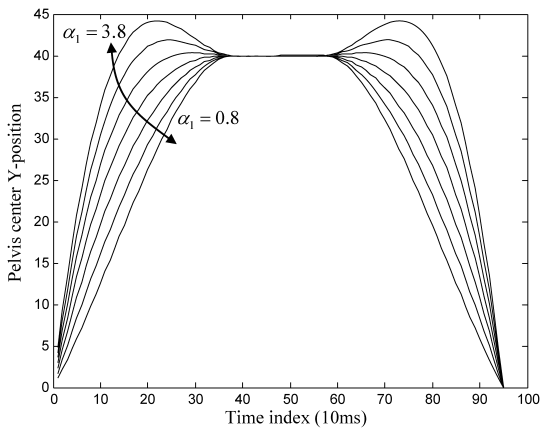

(b)

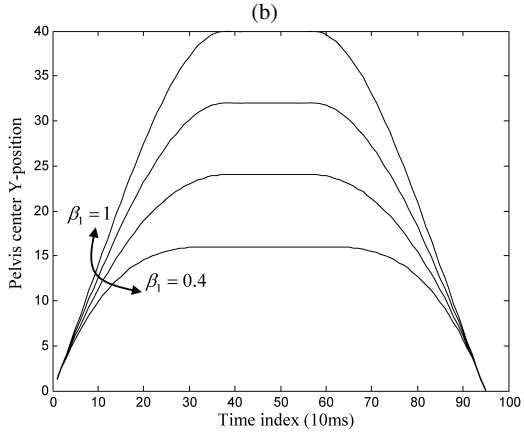

(c)

Figure 15. Example of the changing shape of the Y-position trajectory for the center of the pelvis. (a) Shape change with d_1. (b) Shape change with α_1. (c) Shape change with β_1.

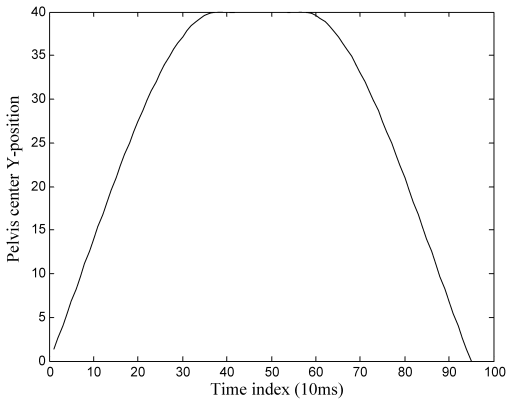

Figure 16. Example of the Y position for the center of the pelvis (for forward walking) (Y-direction: $V_y = 100$, $S_y = 40$ mm, $d_1 = 0.2$).

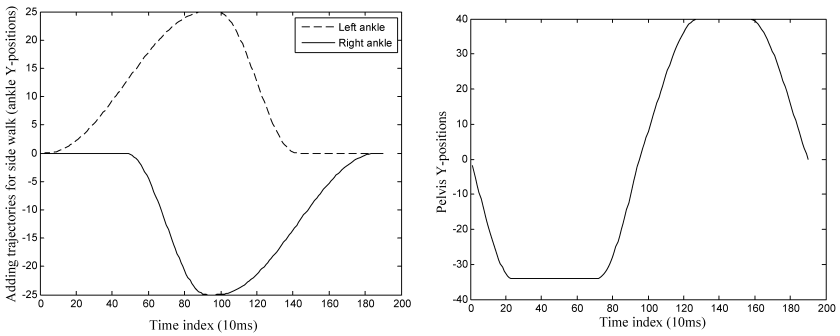

(a) (b)

Figure 17. Trajectory of ankles and the center of the pelvis for the Y position (for left side walking) (length of a side step: 5 cm; open stance stage: $\alpha_1 = 0.85$, $\beta_1 = 0.85$, $d_1 = 0.5$, $V_y = 100$ and $S_y = 40$ mm; recovering stage: $\alpha_1 = 1$, $\beta_1 = 1$, $d_1 = 0.3$, $V_y = 100$ and $S_y = 40$ mm). (a) Additive ankle positions. (b) Position of the center of the pelvis.

function given in (21)–(23) is used:

$$\theta_{\text{Left\_Hip\_Yaw}} = \frac{\theta}{4}\left(1 - \cos\left(\pi \frac{t - t_1^1}{t_2^1 - t_1^1}\right)\right) \tag{21}$$

$$\theta_{\text{Left\_Hip\_Yaw}} = \frac{\theta}{4}\left(1 + \cos\left(\pi \frac{t - t_1^2}{t_2^2 - t_1^2}\right)\right) \tag{22}$$

$$\theta_{\text{Right\_Hip\_Yaw}} = -\theta_{\text{Left\_Hip\_Yaw}}. \tag{23}$$

3.4. Verification of the Walking Pattern With a Simplified ZMP Equation

The simplified ZMP trajectory curves that were induced by the boundary conditions of the trajectory of the center of the pelvis are described in this subsection. The values of the parameters and factors are given in Section 4.2. Figures 20–22

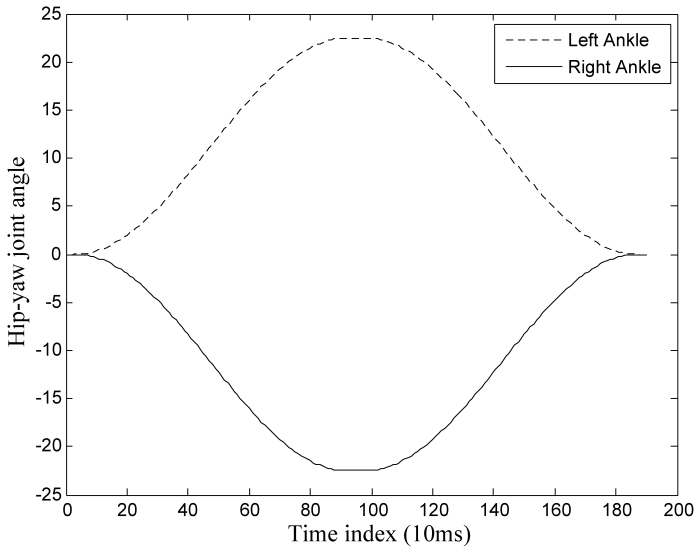

Figure 18. Trajectory of the hip-yaw joint in the turning gait (45° turn).

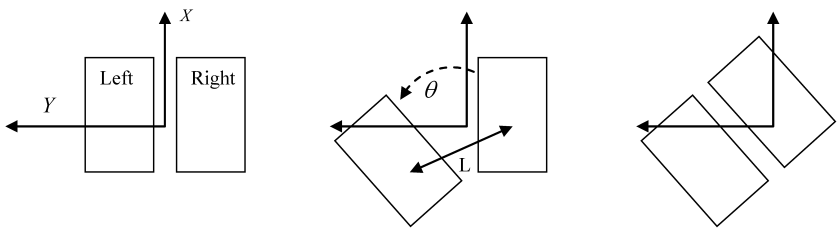

Figure 19. Foot movement of the turning motion.

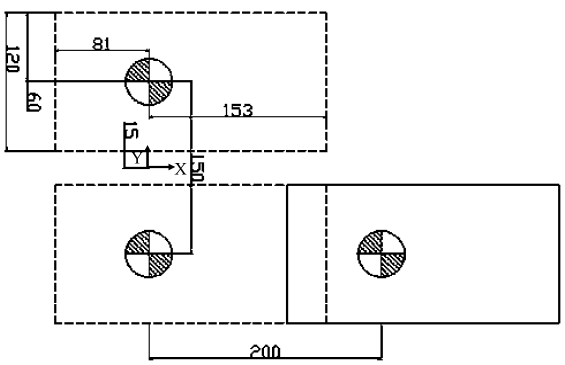

Figure 20. Configuration of the feet (from walking on the spot to a forward step of 20 cm).

show the feet configuration and the desired ZMP trajectories for a forward walking motion that begins with walking on the spot. The forward walking conditions are a

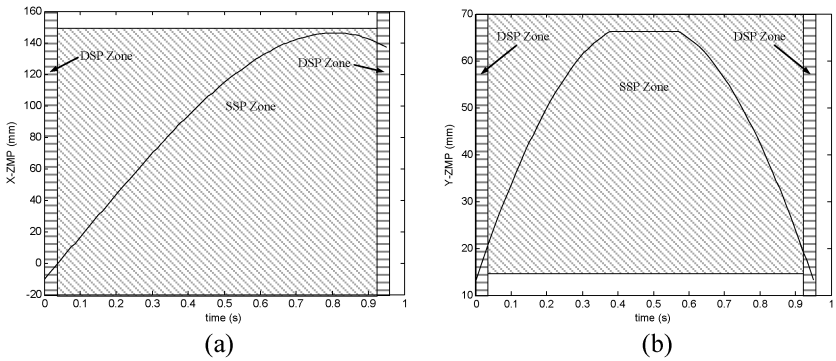

Figure 21. ZMP trajectories with time. (a) X-ZMP. (b) Y-ZMP.

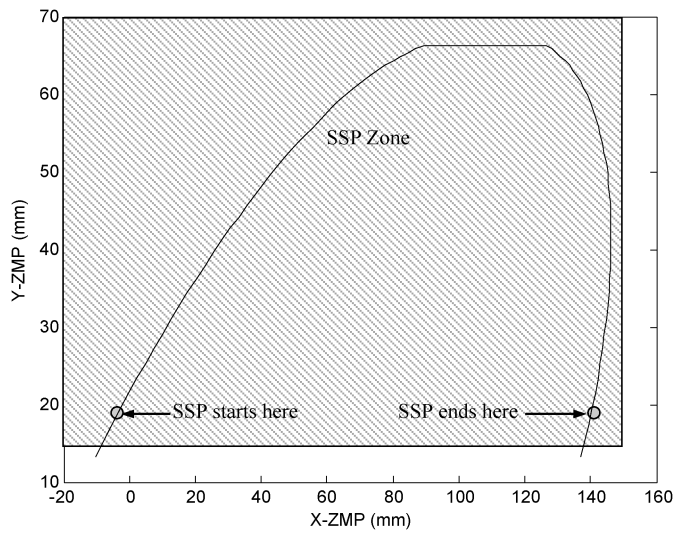

Figure 22. X–Y ZMP trajectory.

step time of 0.95 s and a step length of 20 cm. In this example, the ZMP trajectories are in the supporting area (for the DSP and the SSP) of the robot.

4. Experiments

4.1. Overview of the Robot Platform

The biped humanoid robot KHR-3 (HUBO), which is shown in Fig. 23, is 125 cm tall, weighs 55 kg and has a total of 41 d.o.f. (12 d.o.f. in the legs, 8 d.o.f. in the arms, 6 d.o.f. in the head, 14 d.o.f. in the hands and 1 d.o.f. in the trunk). For the main controller hardware, a Pentium III 933 MHz embedded PC with a Windows XP operating system (OS) and real-time extension (RTX) was used. As Windows XP is a common OS, it is easy for a developer to access and handle, and can easily

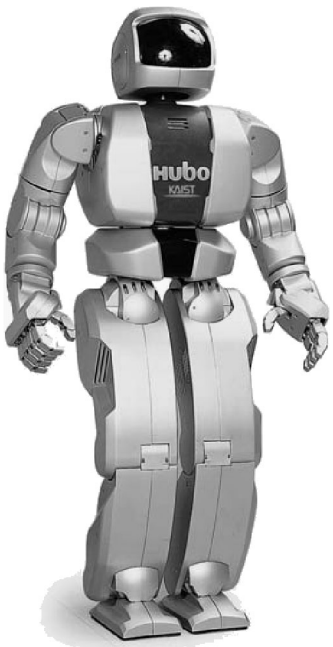

Figure 23. Humanoid robot platform KHR-3.

be used with free or commercial software and hardware drivers. However, although these advantages can reduce the development time and software cost, Windows XP is not a real-time OS; thus, the RTX software was installed on the OS for real-time capability. The RTX software enabled the development of the control software in a familiar environment. The operating environment for the robot and the graphical user interface were developed in the Windows XP environment, and the control algorithm software, which should be executed in real-time, was developed in the RTX environment. Also developed was a 400 W servo controller, which controls the joint DC motors that track the trajectory of the reference position.

The sensory devices, shown in Fig. 24, are as follows: two CCD cameras in the head, force/torque sensors at the ankles and wrists, inclinometers with accelerometers at the soles, and an inertial sensor system in the torso. The servo controller, the sensory devices and the main controller are connected by a two-wired communication line known as a controller area network (CAN). The architecture of the hardware system is shown in Fig. 25. Distributed control architecture with CAN communications was adopted in order to reduce the computation burden, and to allow for easy maintenance, expansion and upgrading of the hardware system. The mechanism of the DC motor/harmonic drive reduction gear was designed as an actuator. The use of a pulley–belt mechanism gave the joint actuator an optimized reduction ratio, as well as minimal uncertainty from factors such as backlash, as the harmonic drive has almost zero backlash. A wireless local area network (LAN) was

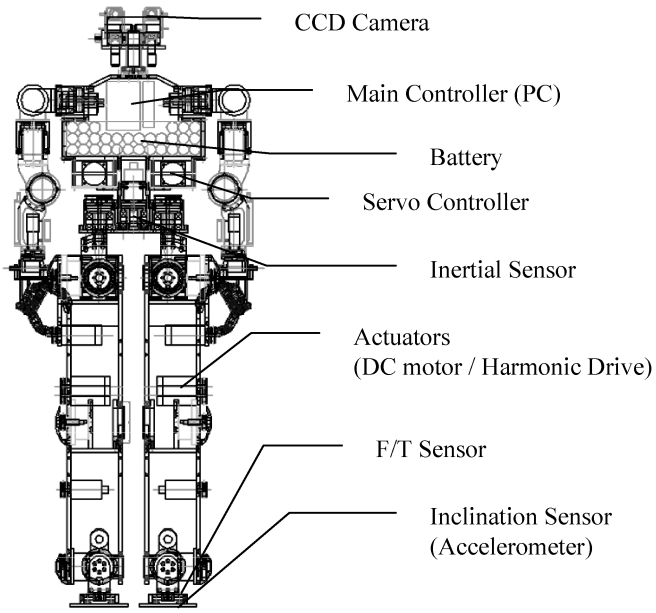

Figure 24. System structure of the KHR-3 hardware.

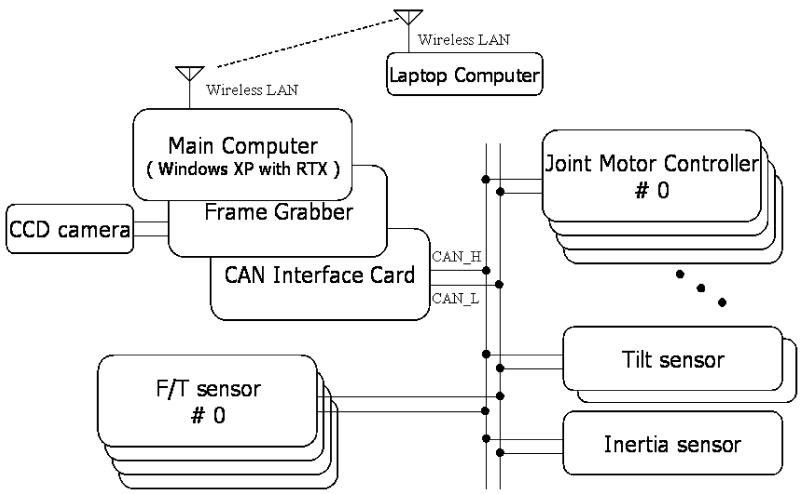

Figure 25. System architecture of the KHR-3.

adopted to operate the robot. Table 1 shows an overview of the specifications of the experimental platform.

4.2. Experimental Results (Application of the Walking Pattern)

Experimental tests were conducted and the capability of the dynamic walking algorithm of KHR-3 was verified. The floor was flat and hard, and the surface had a large amount of friction with the soles to reduce slippage.

Table 1.
Specification's of KHR-3 (Fig. 26)

Research term	January 2004.1–
Weight	55 kg
Height	125 cm
Walking speed	1.25 km/h (previous) → speed variable (1.29 km/h max. now)
Walking cycle and stride	0.95 s/step, 64 cm (previous) → frequency and stride variable (now)
Actuator	servo motor + harmonic reduction gear + drive unit
Control unit	walking control unit, servo control unit, sensor communication unit, communication unit
Sensors	
foot	three-axis force torque sensor and two-axis inclinometer
torso	inertial sensor (three-axis rate gyro and two-axis accelerometer)
Power section	
battery	NiMH battery (24 V/3.3 Ah – 2EA, 12 V/6.6 Ah)
external power	12 V, 24 V (battery and external power supply changeable)
Operating section	laptop computer with wireless LAN
OS	Windows XP and RTX
Degree of freedom	41 d.o.f.

Table 2.
Parameters and shape factors for the walking pattern of forward walking (x: arbitrary value; $d_1 = 0.2$, $\alpha_1 = \beta_1 = 1.0$)

Step time (s)	Step length (cm)	S_y (mm)	α	u
0.95	0	38	x	0.47
	10		1.85	
	20			
	30	39		
0.8	0	35	x	
	10		1.7	
	20		1.6	
	25		1.6	
0.7	0	32	x	0.5
	10		1.7	0.425
	20		1.6	
	25		1.55	

As mentioned in Section 3, the algorithm used to generate the walking pattern has various factors and parameters for walking, the values of which are given in Tables 2 and 3. These values were calculated by means of a simplified ZMP equation and experiments without changing the feedback controller gain. The controllers

Table 3.
Parameters and shape factors for the walking pattern of side walking (the superscript of d_1: 1 is an open stance and 2 is a recovering stance)

Step time (s)	Step length (cm)	S_y (mm)	u	α_1	β_1	$d_1^1 \rightarrow d_1^2$	
0.95	5	38	0.47	0.87	0.87	0.25	0.2
	7			0.85	0.85		
0.8	5	35		0.8	0.8	0.22	0.18
	7				0.78	0.23	0.16
0.7	5	31.5			0.8	0.25	0.12
	7						

are primarily linear controllers, and they are limited with respect to modeling and control action as they are based on simplified models [17–21]. The parameters and factors pertaining to the stability of the walking pattern result in a well-posed and stable walking robot. The parameters and factors for each walking condition (i.e., the step time and step length inputs of an operator) and for each mode (forward/side walking and turning around) were updated on a case-by-case basis for consecutive walking with a variable stride and frequency.

The inputs for the walking motion are the step time, step length for forward walking and step length for side walking. The parameters are the pelvis-Y sway magnitude (S_y) and the velocity (V_y). The factors are α, α_1, β_1 and d_1. Of these factors, α, α_1 and β_1 are described by a multiplier form, and d_1 represents the staying ratio of the pelvis movement. These parameters and factors are vital for generating the desired ZMP trajectory and physically affect the walking performance.

The X-ZMP trajectory of the pelvis is determined by the inputs of the step length and the step time, as well as the α factor. The α factor determines the velocity of the pelvis-X trajectory at the start and end of a step. If the α value is small, the pelvis velocity is slow at the start and the end, but fast in the swinging stage. In contrast, if α is large, the pelvis velocity is quick at the start and the end, but slow in the swinging stage. The pelvis speed depends not only on the α factor, but also on the step length, as the boundary condition related to the pelvis speed is αb and αf. This condition is feasible because the step length becomes longer whenever a faster start/end movement of the pelvis is required with respect to the input step time. If the value of α is not acceptable for walking, the robot falls forward or backward or the pelvis movement has an undesirable acceleration in the X-direction.

The value of V_y defines the pelvis-Y velocity when the step changes (e.g., when the left foot lands on the ground and the right foot starts lifting up, and *vice versa*). It was assumed that the value of V_y was constant and that the boundary condition could be modified by α_1. In addition, α_1 was used to adjust the value of each walking condition, such as the time or stride variation and the forward or side walking mode. When α_1 is small, the pelvis speed at the step change stage is slow. This

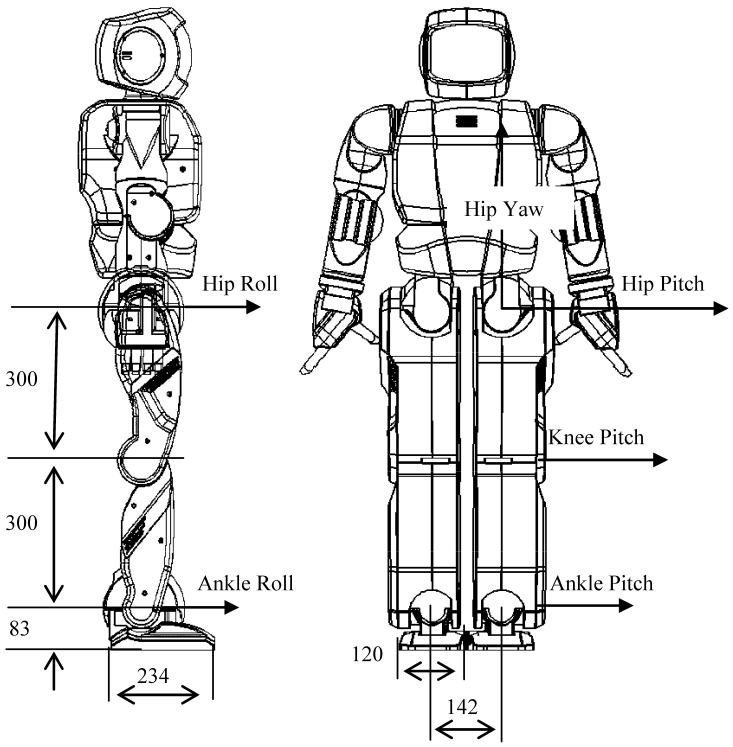

Figure 26. Dimensions and joint axes (units: mm).

situation causes two problems. The first is that the posture of the torso inclines to the inside of the supporting leg. When the lifting leg lands on the ground, the landing shock increases on the landing foot, thereby causing serious instability for the walking motion. The second problem is that an inflection point in the trajectory can arise. The inflection causes a sign change of the acceleration and generates unwanted inertial force in the pelvis. As a result, the induced torso vibration, which is caused by an unacceptable level of inertial force, disrupts the stability of the walking motion. When $\alpha_1 V_y$ is excessively large, the trajectory suffers an unacceptable reverse action. This action should always be taken into account. In this situation, another inflection point has a more deleterious effect on the stability of the robot. The value of S_y determines the position of the pelvis when the foot is lifted to its highest position. This parameter can also be offset by β_1 for the various walking conditions. When S_y is small, the torso inclines to the inside of the supporting foot in the swinging stage. In other situations, the robot tilts over to the outside of the supporting foot. The design of the Y-ZMP trajectory depends on the values of V_y, α_1, S_y and β_1.

The experiments verify that biped walking can be realized by using the proposed method of generating walking patterns; the method relies on a position trajectory framework and proper values of the parameters and factors of each case.

Figures 27–31 show the ZMP data for each case. Figure 27 shows the experimental results for a fixed step time (0.7 s), a variable step length ($0 \rightarrow 10 \rightarrow 20 \rightarrow 25 \rightarrow 0$ cm) and a continual forward walking motion; the parameter and factor val-

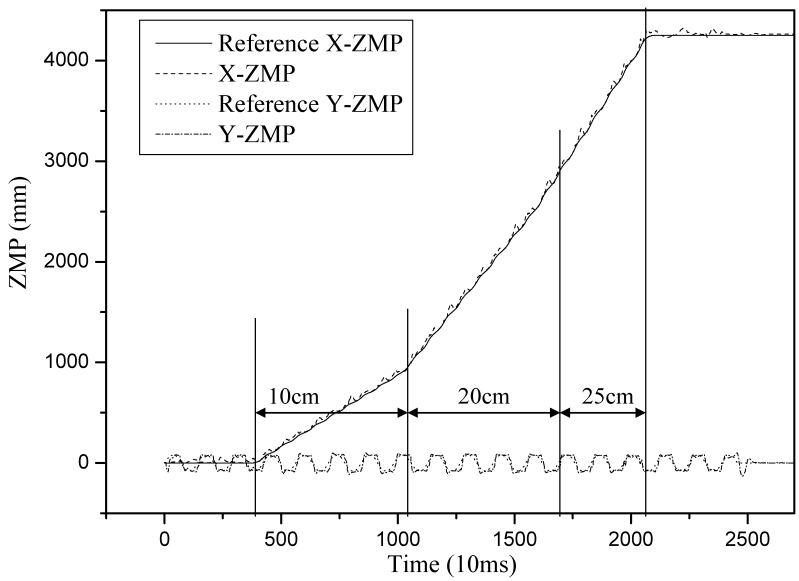

Figure 27. Desired (reference) ZMP and sensor data (forward walking: 0.7 s step time, variable step length).

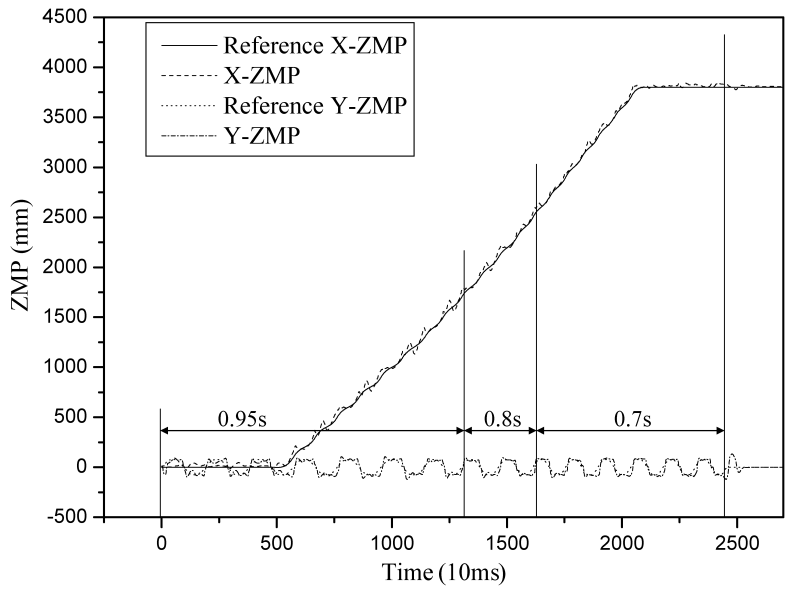

Figure 28. Desired (reference) ZMP and sensor data (forward walking: variable step time, 20 cm step length).

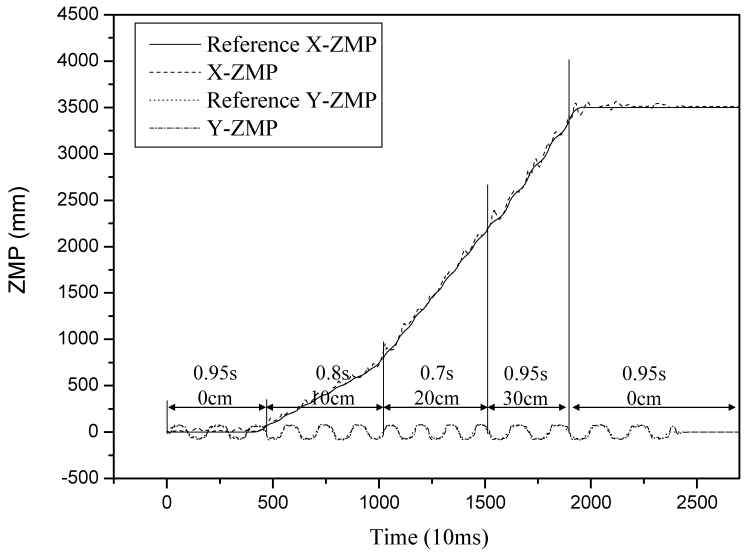

Figure 29. Desired (reference) ZMP and sensor data (forward walking: variable step time, variable step length).

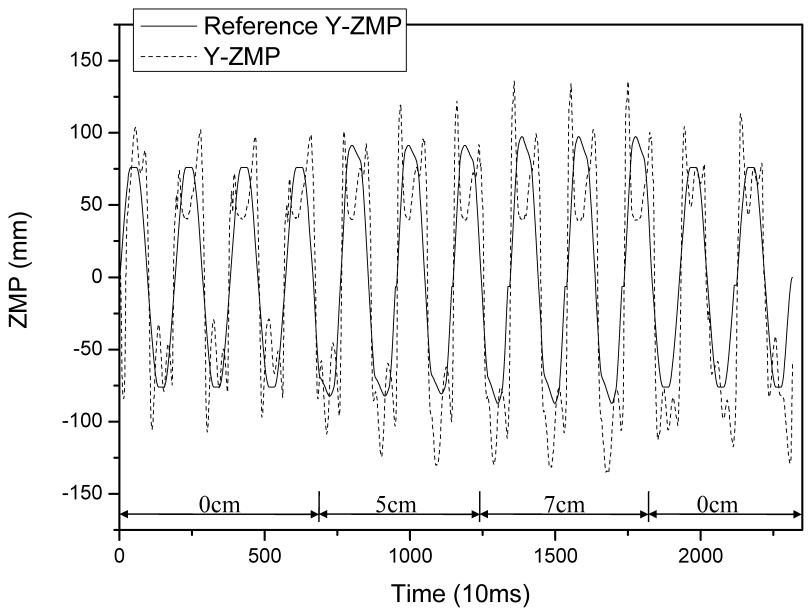

Figure 30. Desired (reference) ZMP and sensor data (side walking: 0.95 s step time, variable step length).

ues are given in Table 2. Figure 28 shows that the robot can change its step time (0.95 → 0.8 → 0.7 s) with a fixed step length (20 cm). The robot walked on the spot for 0.95 s and then moved forward with a variable step time (0.95 → 0.8 → 0.7 s);

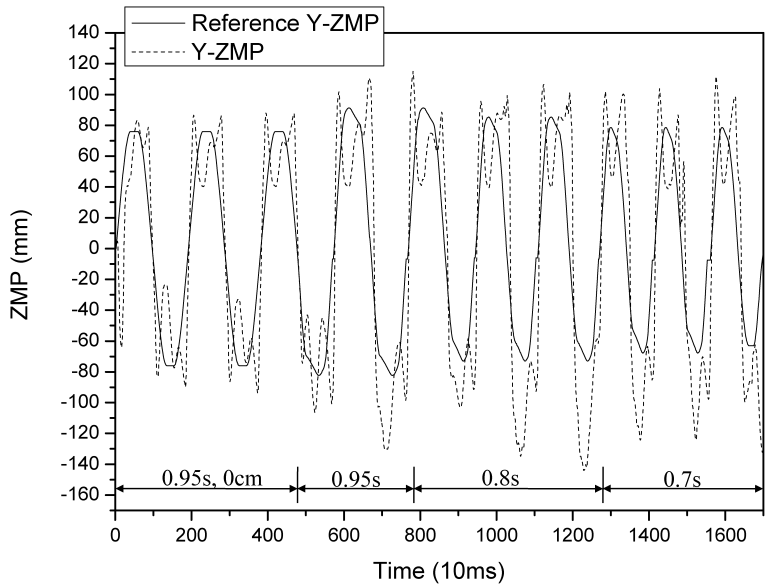

Figure 31. Desired (reference) ZMP and sensor data (side walking: variable step time, 5 cm step length).

it then walked on the spot again for 0.7 s and stopped. With the experiments, the robot was able to change its walking frequency and stride simultaneously, as shown in Fig. 29. Figure 30 shows that the robot can walk sideways with a step time of 0.95 s and a variable side step length ($0 \rightarrow 5 \rightarrow 7 \rightarrow 0$ cm). The side step length denotes the increased distance between the feet when the robot moves from a ready posture to an open-stance posture. The robot can change its walking frequency with a fixed stride condition, as shown in Fig. 31, and it can simultaneously change the frequency and the stride in the side walking mode. Figure 32 shows the walking pattern trajectories with respect to the origin of the center of the pelvis. The ZMP data confirm the success of the experiment.

The simplified model of ZMP ignores the Z-position, acceleration, moments of inertia and angular acceleration. Those factors cause the errors between the real ZMP and the reference ZMP, including the landing shock of the robot. This is the limitation of the proposed approach. However, it is possible to use the proposed method to estimate or design the main tendency of the ZMP trajectory simply and effectively. Furthermore, as mentioned at the beginning of this section and in Section 1, errors can be offset using feedback controllers.

5. Conclusions and Future Work

A simple and effective on-line scheme for generating a biped walking pattern is proposed in this paper. The pattern generation scheme is based on the generation of task-level commands with inputs pertaining to the step time, stride and direction.

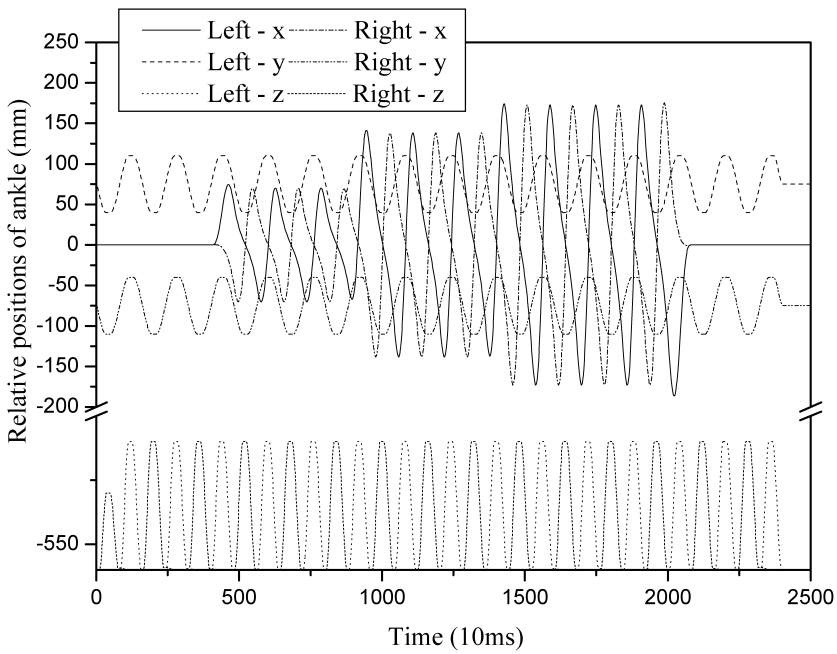

Figure 32. Relative walking pattern trajectories with respect to the pelvis center origin (forward walking: 0.8 s step time, variable step length).

The pattern is composed of smooth curves and the superposition of those curves. The requirement for the smoothness of the position trajectory is for an actual implementation.

For the trajectory of the pelvis, third-order polynomial interpolation is proposed as this is commonly used for the pelvis curve in other research. However, a new aspect of this method is the generation of the desired ZMP trajectory by means of an update of the boundary condition and a direct one-to-one relationship with the pelvis trajectory. The scheme was verified *via* experimentation.

The requirements of the pattern generation method are discussed at the beginning of Section 3. The pattern uses inputs, parameters and shape factors, most of which are related to the pelvis and position trajectories such as the amplitude of the sway and the velocity at the beginning and end of each step. By updating the boundary conditions at every step, the variable stride and frequency of the biped walking motion is realized. This updating strategy, which is based on effective parameters and organizational factors of walking, facilitates the extraction of independent parameters and factors (the center position and velocity of the pelvis).

To estimate the optimal parameters and factors for each walking condition and mode, the relationship between the desired ZMP equation and the trajectory of the center of the pelvis was used, as mentioned in Section 2. The fine tuning of the values was completed through experiments.

Flexible biped walking was realized in terms of the step time, stride and mode. The proposed method of pattern generation enhances the walking speed and flexibility of the robot. It was found, for example, that the walking speed accelerated when the speed of the frequency or stride was increased. The significance of this method is that it is now possible to conduct effective experiments with various step times and strides. Simple and easily tunable, the proposed method of generating a trajectory facilitates the realization of various walking conditions (inputs).

In the near future, the authors intend to determine the shape factors and parameter values automatically and adaptively using various criteria such as the ZMP and the attitude for arbitrary walking situations. A scheduling method will also be utilized for the untested intermediate walking conditions (inputs), which will allow these factors and values to be determined.

The boundary conditions consider the position and the velocity of the pelvis center. With the proposed scheme, the order of polynomial can easily be increased to include acceleration as well as the jerk of the pelvis trajectory in the boundary condition. This scheme will be upgraded to take into account the acceleration and the jerk of the ZMP or the pelvis center.

Inaccuracies in the model can be caused by other values not considered in this paper, such as the Z-position/acceleration, moments of inertia and angular accelerations. To expand the proposed scheme, more consideration shall be given to the values from a practical and effective point of view.

References

1. J. Yamaguchi, A. Takanishi and I. Kato, Development of a biped walking robot compensating for three-axis moment by trunk motion, in: *Proc. IEEE/RSJ Int. Conf. on Intelligent Robots and Systems*, Yokohama, pp. 561–566 (1993).
2. K. Hirai, Current and future perspective of Honda humanoid robot, in: *Proc. IEEE/RSJ Int. Conference on Intelligent Robots and Systems*, Grenoble, pp. 500–508 (1997).
3. K. Hirai, M. Hirose, Y. Haikawa and T. Takenaka, The development of Honda humanoid robot, in: *Proc. IEEE Int. Conf. on Robotics and Automations*, Leuven, pp. 1321–1326 (1998).
4. K. Kaneko, F. Kanehiro, S. Kajita, K. Yokoyama, K. Akachi, T. Kawasaki, S. Ota and T. Isozumi, Design of prototype humanoid robotics platform for HRP, in: *Proc. IEEE Int. Conf. on Intelligent Robots and Systems*, EPFL, Lausanne, pp. 2431–2436 (2002).
5. K. Nishiwaki, T. Sugihara, S. Kagami, F. Kanehiro, M. Inaba and H. Inoue, Design and development of research platform for perception–action integration in humanoid robot: H6, in: *Proc. IEEE/RSJ Int. Conf. on Intelligent Robots and Systems*, Takamatsu, pp. 1559–1564 (2000).
6. K. Kaneko, *et al.*, Design of LRP humanoid robot and its control method, in: *IEEE Int. Workshop on Robot and Human Interactive Communication*, Bordeaux, pp. 556–561 (2001).
7. Y. Sakagami, R. Watanabe, C. Aoyama, S. Matsunaga, N. Higaki and K. Fujimura, The intelligent ASIMO: system overview and integration, in: *Proc. IEEE/RSJ Int. Conf. on Intelligent Robots and Systems*, EPFL, Lausanne, pp. 2478–2483 (2002).
8. K. Kaneko, F. Kanehiro, S. Kajita, H. Hirukawa, T. Kawasaki, M. Hirata, K. Akachi and T. Isozumi, Humanoid robot HRP-2, in: *Proc. IEEE Int. Conf. on Robotics and Automation*, New Orleans, LA, pp. 1083–1090 (2004).

9. C. L. Shih, Y. Z. Li, S. Churng, T. T. Lee and W. A. Cruver, Trajectory synthesis and physical admissibility for a biped robot during the single support phase, in: *Proc. IEEE Int. Conf. Robotics and Automation*, Cincinati, OH, pp. 1646–1652 (1990).
10. T. G. McGee and M. W. Spong, Trajectory planning and control of a novel walking biped, in: *Proc. IEEE Int. Conf. Control Applications*, Mexico City, pp. 1099–1104 (2001).
11. Q. Huang, K. Yokoi, S. Kajita, K. Kaneko, H. Arai and N. Koyachi, Planning walking patterns for a biped robot, *IEEE Trans. Robotics Automat.* **17**, 280–289 (2001).
12. H. Lim, Y. Kaneshima and A. Takanishi, Online walking pattern generation for biped humanoid robot with trunk, in: *Proc. IEEE Int. Conf. on Robotics and Automation*, Washington, DC, pp. 3111–3116 (2002).
13. S. Kagami, K. Nishiwaki, T. Kitagawa, T. Sugihiara, M. Inaba and H. Inoue, A fast generation method of dynamically stable humanoid robot trajectory with enhanced ZMP constraint, in: *Proc. of IEEE Int. Conf. on Humanoid Robotics*, Boston, MA (2000).
14. S. Kajita, F. Kanehiro, K. Kaneko, K. Fujiwara, K. Yokoi and H. Hirukawa, A real-time pattern generator for biped walking, in: *Proc. IEEE Int. Conf. Robotics and Automation*, Washington, DC, pp. 31–37 (2002).
15. S. Kajita, F. Kanehiro, K. Kaneko, K. Fujiwara, K. Harada, K. Yokoi and H. Hirukawa, Biped walking Pattern generation by using preview control of zero-moment point, in: *Proc. IEEE Int Conf. on Robotics and Automation*, Taipei, pp. 1620–1626 (2003).
16. M. Morisawa, S. Kajita, K. Kaneko, K. Harada, F. Kanehiro, K. Fujiwara and H. Hirukawa, pattern generation of biped walking constrained on parametric surface, in: *Proc. IEEE Int. Conf. on Robotics and Automation*, Barcelona, pp. 2405–2410 (2005).
17. J. H. Kim and J. H. Oh, Realization of dynamic walking for the humanoid robot platform KHR-1, *Adv. Robotics* **18**, 749–768 (2004).
18. J. Y. Kim, I. W. Park and J. H. Oh, Design and walking control of the humanoid robot, KHR-2, in: *Proc. Int. Conf. on Control, Automation and Systems*, Bangkok, pp. 1539–1543 (2004).
19. J. Y. Kim, I. W. Park, J. Lee, M. S. Kim, B. K. Cho and J. H. Oh, System design and dynamic walking of humanoid robot KHR-2, in: *Proc. IEEE Int. Conf. on Robotics and Automation*, Barcelona, pp. 1443–1448 (2005).
20. J. Y. Kim, I. W. Park and J. H. Oh, Vibration reduction control for human-riding biped robot HUBO FX-1, in: *Proc. IEEE Int. Federation of Automation & Control*, Heidelberg (2006).
21. J. Y. Kim, I. W. Park and J. H. Oh, Experimental realization of dynamic walking of biped humanoid robot KHR-2 using ZMP feedback and inertial measurement, *Adv. Robotics* **20**, 707–736 (2006).

About the Authors

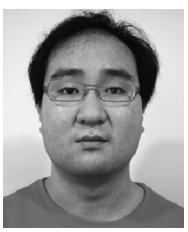

Ill-Woo Park received the BS and MS degrees in Mechanical Engineering from the Korea Advanced Institute of Science and Technology (KAIST), Daejeon, South Korea, in 2000 and 2002, respectively. He is currently a Graduate Student of the PhD course in the Department of Mechanical Engineering at KAIST. His research interests include humanoid robot design and biped walking control.

Jung-Yup Kim received the BS and MS degrees in Mechanical Engineering from INHA University, Incheon, South Korea, and the PhD degree in Mechanical Engineering from Korea Advanced Institute of Science and Technology (KAIST), in 1999, 2001 and 2006, respectively. He is currently a Post-Doc in the Department of Mechanical Engineering at KAIST. His research interests include the design and control of biped humanoid robots, visual processing using CCD cameras, development of sensory devices using micro-processor, and tele-operating systems. He is a Member of the KSME and ICASE.

Jun-Ho Oh received the BS and MS degrees in Mechanical Engineering from Yonsei University, Seoul, South Korea, and PhD degree in Mechanical Engineering from the University of California, Berkeley, CA, USA, in 1977, 1979 and 1985, respectively. He was a Researcher with Korea Atomic Energy Research Institute, from 1979 to 1981. Since 1985, he has been with Department of Mechanical Engineering, Korea Advanced Institute of Science and Technology, where he is currently a Professor. He was a Visiting Research Scientist at the University of Texas Austin from 1996 to 1997. His research interests include humanoid robots, adaptive control, intelligent control, nonlinear control, biomechanics, sensors, actuators and the application of micro-processors. He is a Member of the IEEE, KSME, KSPE and ICASE.